

**Initial growth of Ba on Si(001)**Anthony J. Ciani,<sup>1</sup> Prasenjit Sen,<sup>2</sup> and Inder P. Batra<sup>1,\*</sup><sup>1</sup>*Department of Physics, University of Illinois at Chicago, Chicago, Illinois 60607, USA*<sup>2</sup>*Department of Physics, North Carolina State University, Raleigh, North Carolina 27695, USA*

(Received 18 December 2003; published 15 June 2004)

We have studied the formation of stable Ba structures on the Si(001) surface, from sparse coverage up to one monolayer (ML) coverage, using density-functional theory based total-energy calculations employing pseudopotentials. At sparse coverage Ba has the highest binding energy at the valley bridge site (center of four Si dimers). As the coverage increases, Ba bonds at valley bridge sites neighboring previously adsorbed Ba atoms, leading to the possibility of Ba chain formation between the rows of Si dimers. At  $\frac{1}{3}$  ML coverage we confirm the stability of the ordered  $(2 \times 3)$  phase which has been observed in many experiments. As the coverage increases beyond  $\frac{1}{3}$  ML, the hollow site (on the dimer rows between two dimers) is preferentially occupied. Tests of configurations with  $(2 \times 1)$  through  $(2 \times 6)$  symmetries at  $\frac{1}{2}$  ML coverage showed that Ba atoms are stabilized in a mixture of hollow and valley bridge sites, forming a 2D pattern of interrupted chains of 2–5 Ba atoms running between the dimer rows, with several symmetries nearly degenerate. Only some of these  $(2 \times N)$  structures have been reported in experiments;  $(2 \times 1)$ ,  $(2 \times 3)$ ,  $(2 \times 4)$ , and  $(2 \times 6)$ . The near degeneracy of these  $(2 \times N)$  structures may be the reason for the poor periodicity observed in some experiments. We tested the periodicity across the dimer rows and found that the pattern of Ba atoms in one valley should repeat in the next, creating a  $2 \times$  symmetry. At one monolayer coverage, Ba atoms on the surface do not form Ba-Ba dimer bonds, nor do they break the surface Si dimers.

DOI: 10.1103/PhysRevB.69.245308

PACS number(s): 68.43.Bc, 68.43.Fg

**I. INTRODUCTION**

Barium is important for various Si based technological applications. Alkali metals, in general, are known to reduce the work function of the silicon surface and are used in electron emitters. Barium can be used to form a buffer layer between Si and elements too reactive with Si to be grown in direct contact with Si. The use of Ba as an intermediate layer between Si and Ba containing materials, particularly Ba based insulators and high- $T_C$  superconductors has also been suggested. It is important to investigate the geometrical arrangements of the Ba overlayer since this determines the growth characteristics of the subsequent layers used in device fabrication. There is also interest in finding metallic adsorbates which might be used in the formation of stable, atomic scale, metallic interconnects. Hence the adsorption of Ba from submonolayer to one monolayer coverage on Si(001)- $p(2 \times 1)$  is an important topic of study.

One monolayer coverage of Ba occurs when there is one Ba adsorbate per Si surface atom, which on Si(001) occupies an area  $3.84 \times 3.84 \text{ \AA}^2$ , and corresponds to a surface density of  $6.78 \times 10^{14} \text{ cm}^{-2}$ . To date, many low-energy electron diffraction (LEED) studies<sup>1–6</sup> have found that the Ba covered surface can have  $(2 \times 1)$ ,  $(2 \times 3)$ ,  $(2 \times 4)$ , and  $c(2 \times 6)$  phases, dependent on Ba coverage and substrate temperature. Urano<sup>4</sup> showed that these phases exist with the “2” part of the symmetry perpendicular to the dimer rows.

Many scanning tunneling microscope (STM) studies<sup>7–11</sup> have indicated a lack of long-range periodicity (except at  $\frac{1}{3}$  ML coverage), and have provided good information about the topology of the surface. Barium chains running across the dimer rows have been observed with the STM (Ref. 8) at less than  $\frac{1}{3}$  ML, although Wang *et al.*<sup>14</sup> predicted the formation of these chains along the dimer rows. Knowledge about

the geometry of the surface has also been provided by x-ray standing wave<sup>12</sup> and coaxial impact ion scattering<sup>13</sup> experiments. To the best of our knowledge, only one density-functional calculation<sup>14</sup> has been performed, which identified the preferred binding sites, bonding nature, and diffusion rates at  $\frac{1}{16}$  ML coverage.

Most studies have found that at low coverage Ba bonds primarily at the valley bridge site,<sup>7–15</sup> and that as coverage increases Ba starts binding on a second site.<sup>7–9,12,13,15</sup> Although there is some disagreement as to which site this is, most work points to the hollow site.<sup>7,13,14</sup> Our goal in this paper is to identify the stable energy structures from  $\frac{1}{16}$  up to 1 ML.

We address these questions with the use of density-functional based total-energy pseudopotential calculations. The energies at special symmetric binding sites at various coverages, the experimentally suggested structures, and some other possible structures are investigated. These energies and the resulting structures are then used to provide an explanation of the experimentally observed structures.

**II. METHOD**

Calculations were performed using density functional theory (DFT) in the pseudopotential framework. The commercial package VASP (Refs. 16,17) was used for the calculations. The wave functions are expressed as plane waves with an energy cutoff of 250 eV. The Brillouin zone integrations are performed using the Monkhorst-Pack scheme<sup>18</sup> with the origin shifted to the  $\Gamma$  point. Ionic potentials are represented by ultrasoft Vanderbilt type pseudopotentials,<sup>19</sup> and results for the fully relaxed atomic structures are obtained using the generalized gradient approximation (GGA) (Ref. 20) for the exchange-correlation energy. The H, Si, and

Ba pseudopotentials had  $1s^1$ ,  $3s^23p^2$ , and  $6s^25p^6$  valences, respectively. The preconditioned conjugate gradient method (as implemented in VASP) is used for wave function optimization and conjugate gradient is used for ionic relaxation. We used a  $4 \times 8 \times 1$   $\mathbf{k}$  point mesh for the  $(2 \times 1)$  supercell, a  $4 \times 4 \times 1$   $\mathbf{k}$  point mesh for the  $(2 \times 2)$  supercell, a  $4 \times 3 \times 1$   $\mathbf{k}$  point mesh for the  $(2 \times 3)$ ,  $(2 \times 4)$ , and  $(2 \times 5)$  supercells, a  $4 \times 2 \times 1$   $\mathbf{k}$  point mesh for the  $(2 \times 6)$  supercell, and a  $2 \times 2 \times 1$   $\mathbf{k}$  point mesh for the  $(4 \times 4)$  supercell. The convergence with respect to the energy cutoff and number of  $\mathbf{k}$  points was tested.

The ions in the supercells were relaxed until additional ionic motions caused changes of less than 5 meV to the total energy of the entire supercell. When making comparisons between the binding energies of different structural arrangements of atoms with the same size supercell, the errors due to cutoff and  $\mathbf{k}$  point mesh tend to cancel.<sup>21</sup> To determine the error among different sized supercells we compared the energies of each size supercell for unrelaxed Si slabs. The largest difference was around 10 meV per  $(2 \times 1)$  unit cell between the  $(2 \times 1)$  supercell and all other sizes. The energy differences among all supercells other than the  $(2 \times 1)$  supercell were less than 1 meV per  $(2 \times 1)$  unit cell, which is generally smaller than the error introduced by the relaxation criteria.

The Si(001)- $p(2 \times 1)$  surface is represented by a repeated slab geometry. Each slab contains 5 Si atomic layers with hydrogen atoms passivating the Si atoms at the bottom layer of the slab. Consecutive slabs are isolated from each other by a vacuum space of 12 Å. The Si atoms in the top four atomic layers are allowed to relax, while the bottom layer Si atoms and passivating H atoms are fixed to simulate bulklike termination. We reproduced the energetics and geometry of the  $p(2 \times 1)$  reconstructions of a clean Si(001) surface using the above parameters.<sup>21</sup>

The calculations provide the cohesive energy of the supercell composed of the given constituent atoms,

$$E_C[\text{SC}] = E_T[\text{SC}] - E_A[\text{atoms}], \quad (1)$$

where  $E_C[\text{SC}]$  is the cohesive energy of the supercell,  $E_T[\text{SC}]$  is the total energy (Hartree, Ewald, exchange-correlation, eigenvalues, etc.) of the supercell, and  $E_A[\text{atoms}]$  is the energy of the isolated atom for each atom in the supercell, thus  $E_C[\text{SC}]$  is the energy gained by assembling the structure given by the supercell from the isolated atoms. We define the binding energies  $E_B$  as,

$$E_B = E_C[\text{Si}] - E_C[\text{Si} + n\text{Ba}], \quad (2)$$

where  $E_C[\text{Si}]$  is the cohesive energy of the relaxed Si slab, and  $E_C[\text{Si} + n\text{Ba}]$  is the cohesive energy after relaxation with  $n$  Ba atoms adsorbed onto the slab. The cohesive energies of the slab with and without Ba are calculated in the same supercell with a fully relaxed atomic configuration. The energies given in this paper are the binding energies per Ba adatom,  $E_B/n$ , unless otherwise stated.

It should be noted that when properly treated, the binding energy would be written as

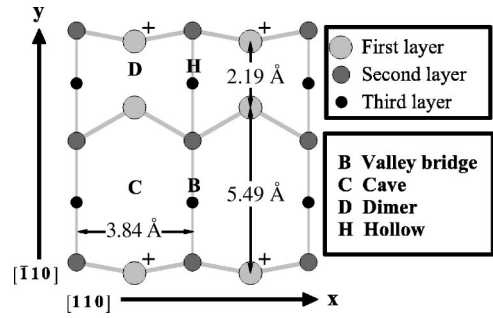


FIG. 1. (Color online) The four symmetry adsorption sites used in our calculations, and the overhead view of the  $p(2 \times 1)$  surface. The Si atoms marked with a “+” are the higher atoms in the Si dimers.

$$E_B = E_C[\text{Si}] - E_C[\text{Si} + n\text{Ba}] + n\mu_{\text{Ba,R}},$$

where  $\mu_{\text{Ba,R}}$  is the chemical potential of a Ba atom in its reference state. We use Eq. (2) because we are making comparisons among supercells with equal numbers of each species, and because  $\mu_{\text{Ba,R}}$  changes with the reference state of Ba. Using the same energy cutoff as our slab calculations, we found the chemical potential of Ba in its bulk bcc phase to be  $\mu_{\text{Ba,R}} = -1.90$  eV.

### III. SPARSE BARIUM COVERAGE

In order to test the parameters described in Sec. II, we calculated the total energy of the  $p(2 \times 1)$  reconstruction of the clean Si(001) surface in a supercell comprising a  $(4 \times 4)$  ideal cell (composed of 80 Si atoms and 32 H atoms). The Si atoms in the top four layers are relaxed to obtain the optimized structure of the surface, while the bottom layer of Si atoms and passivating H atoms are kept fixed to simulate bulk termination. Our results are in good agreement with the earlier density functional calculations.<sup>21</sup> For the  $p(2 \times 1)$  surface with *asymmetric* Si dimers, there is an energy gain of 1.7 eV per dimer. The Si dimer distance is 2.31 Å between nuclei, and the dimer bond makes an angle of 18.9° with the horizontal plane. The optimized atomic positions can be found in a previous paper.<sup>22</sup> Although higher order reconstructions of the Si(001) surface have lower energies,<sup>21</sup> the differences between these and the  $p(2 \times 1)$  reconstruction are small in comparison to the changes caused by the adsorption of adatoms, so we use the  $p(2 \times 1)$  reconstruction for simplicity and uniformity across the different sized supercells [which are multiples of the  $(2 \times 1)$  supercell].

We calculated the binding energies of a single Ba atom adsorbed on four special symmetry sites of the Si(001)- $p(2 \times 1)$  unit cell. These sites are: dimer bridge (D), cave (C), hollow (H), and valley bridge (B) sites shown in Fig. 1.

Calculations were performed using a  $(4 \times 4)$  supercell consisting of eight  $(2 \times 1)$  unit cells. The large size of the supercell ensures that the interactions between an adsorbed Ba atom and its periodic images are negligible, so that results represent an isolated Ba adatom. In Fig. 1, only one  $(2 \times 2)$  cell of the supercell is shown.

TABLE I. Binding energies per adatom (in eV) of Ba adatoms for  $\frac{1}{16}$ ,  $\frac{1}{4}$ , and  $\frac{1}{2}$  ML coverages at special sites. A  $(4 \times 4)$  symmetry was used for the  $\frac{1}{16}$  ML energies, and a  $(2 \times 1)$  symmetry was used for the  $\frac{1}{2}$  ML energies. To obtain the  $\frac{1}{4}$  ML energies we used a  $(4 \times 2)$  symmetry for the **B** and **H** sites instead of a  $(2 \times 2)$  symmetry since at this coverage it is energetically unfavorable to have Ba atoms aligned in the  $[\bar{1}10]$  direction for the **B** and **H** sites. The **C** and **D** sites seem unaffected by this, therefore a  $(2 \times 2)$  symmetry was used to obtain the energies at those sites.

Site	$\frac{1}{16}$ ML	$\frac{1}{4}$ ML	$\frac{1}{2}$ ML
<b>B</b>	4.34	4.18	3.90
<b>H</b>	3.85	3.76	3.38
<b>C</b>	3.42	3.60	2.66
<b>D</b>	3.43	3.09	2.14

The binding energies per Ba adatom are listed in Table I, and the heights of the Ba adatoms and Si dimers above the bulk-projected second Si layer are listed in Table II. In general, the binding energy per adatom decreases as coverage increases, but the energy for the **C** site shows a slight increase initially, and then, a decrease as we go from  $\frac{1}{4}$  ML to  $\frac{1}{2}$  ML. While the initial increase appears to violate the rule, it should be noted that the rule applies to the binding energies of the preferred structures. Although something interesting may be happening at the **C** site, we note that the highest binding energy for each coverage is decreasing with increasing coverage. The site with the highest binding energy at low coverage is the **B** site, where the Ba atom adsorbs between the dimer rows of the clean Si(001)- $p(2 \times 1)$  surface at the center of four Si dimers, and is bonded to the four neighboring Si atoms of the dimers. The next preferred site is the **H** site, above the dimer row. It is worth noting that the binding energy of the Barium atom decreases with coverage.

Barium has a  $6s^2$  valence, and so we should expect that it will nominally bond with two Si surface atoms since each Si surface atom has one dangling bond. However, the  $s$  symmetry means that Ba does not have lobes at which it needs to form bonds, so Ba could bond symmetrically between multiple surface atoms forming metallic or ionic bonds. If we make a comparison to another  $s$ -shell species, Na,<sup>23</sup> we might expect Ba to bond on the **H** or **B** sites, which have four atoms at their corners. In contrast,  $p$ -shell atoms, such as

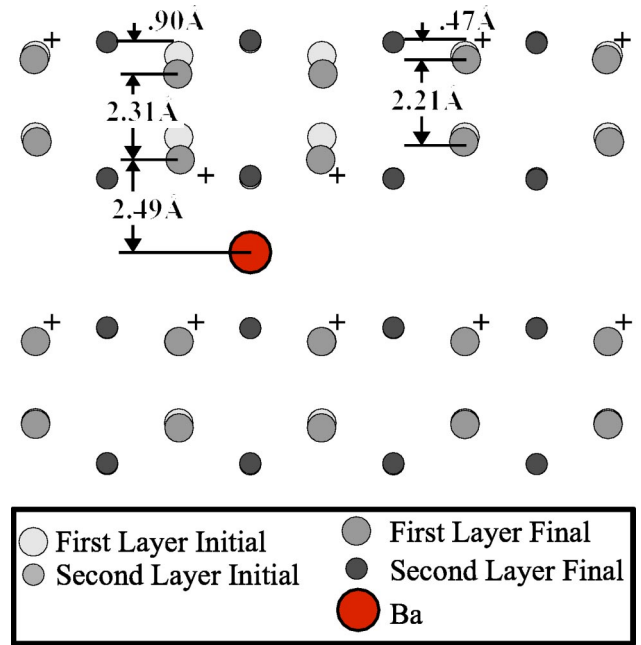


FIG. 2. (Color online) Top view of the **B** site at  $\frac{1}{16}$  ML coverage in a  $(4 \times 4)$  supercell. The higher Si atom in each dimer is labeled with +.

Te,<sup>22</sup> have a lobed symmetry, and bond on the **C** or **D** sites. An adsorbed Ba atom should prefer the **B** site over the **H** site because bonding at the **B** site will require less bending of the dangling bonds, and the dimer bonds can be left intact.

What we see from the energetics is that the **B** site is indeed preferred over the **H** site, which is consistent with our intuitive arguments. Referring to Figs. 2 and 3 we can see a top view of the change the Si surface undergoes as Ba atoms bond on the **B** and **H** sites, respectively. It is important to note that the Ba atoms are not large enough to bond across the **B** site, unless the dimers in one row flip their direction. In Fig. 2 we can see that the dimers above the adsorbed Ba atom have shifted towards the binding site. This shift is accompanied by a flip in the tilt (from  $+18.9^\circ$  to  $-11.7^\circ$ ) of the two dimers, and a slight increase in the heights of the four dimers surrounding the site. The higher Si atoms in the dimers are labeled with “+” in Fig. 2. Looking at the **H** site in Fig. 3 we can see that the Si atoms forming the dimers have been pushed slightly apart, and the two dimers around

TABLE II. Heights (in Å) of the Ba adatoms, Si dimers, and relaxed second Si layer above the bulk projected second Si layer for  $\frac{1}{16}$ ,  $\frac{1}{4}$ , and  $\frac{1}{2}$  ML coverages at special sites, with respective  $(4 \times 4)$ ,  $(2 \times 2)$ , and  $(2 \times 1)$  symmetries. The spacing between bulk layers is 1.36 Å, which comes from dividing the Si lattice constant (5.43 Å) by 4.

Site	$\frac{1}{16}$ ML			$\frac{1}{4}$ ML			$\frac{1}{2}$ ML		
	Ba	Dimer	2nd layer	Ba	Dimer	2nd layer	Ba	Dimer	2nd layer
<b>B</b>	2.77	1.17	0.05	2.53	1.30	0.03	2.54	1.44	0.04
<b>H</b>	3.45	1.16	0.06	3.38	1.22	0.03	3.50	1.32	0.03
<b>C</b>	3.20	1.18	0.06	3.13	1.26	0.05	2.93	1.28	0.01
<b>D</b>	4.14	1.15	0.06	4.09	1.22	0.04	4.06	1.28	0.02

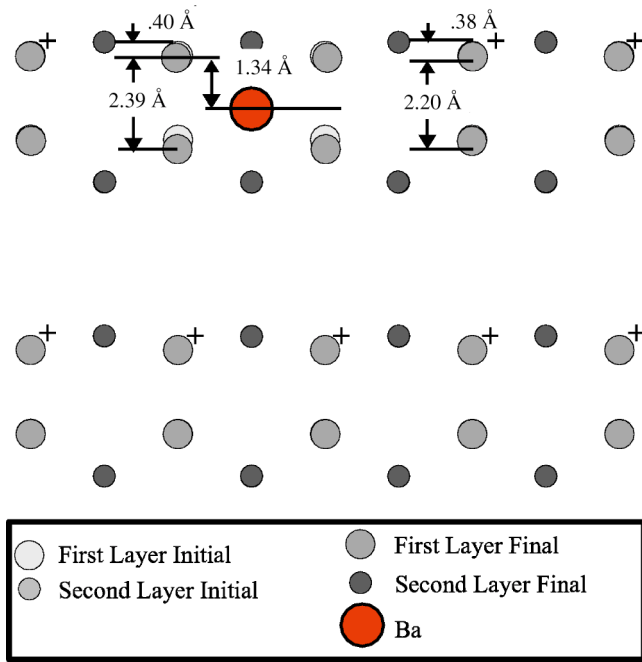


FIG. 3. (Color online) Top view of the **H** site at  $\frac{1}{16}$  ML coverage in a  $(4 \times 4)$  supercell. The higher Si atom in each dimer is labeled with +, when appropriate.

the Ba adatom become symmetric. The distortions associated with bonding on both the **B** and **H** sites are localized around the site. The Ba adatoms have very little effect on the neighboring dimer rows.

The bonding nature of the Ba atoms appears to be ionic. The charge density along the line between an adsorbed Ba atom on a **B** site and one of the neighboring surface Si atoms is shown in Fig. 4. Using  $1.65 \text{ \AA}$  as the radius of the Ba adatom, we can see from Fig. 5 that the adsorbed Ba atom

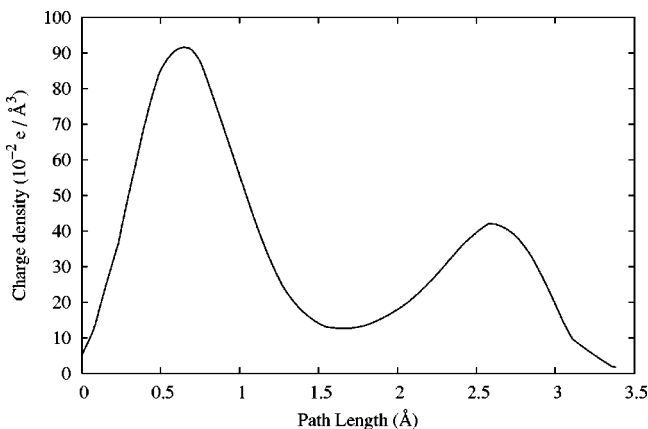


FIG. 4. The charge density along the line between a Ba atom adsorbed at a **B** site at  $\frac{1}{16}$  ML coverage and a neighboring Si surface atom. The unit is hundredths of  $e/\text{\AA}^3$ . The line starts at the nucleus of the Ba atom and ends at the nucleus of the Si atom. The minimum of the charge density between the atoms is about  $1.65 \text{ \AA}$  from the nucleus of the Ba atom. Looking at Fig. 8 it can be seen that this is also the approximate radius of the Ba atom, which is substantially smaller than its atomic radius of  $\sim 2.3 \text{ \AA}$ .

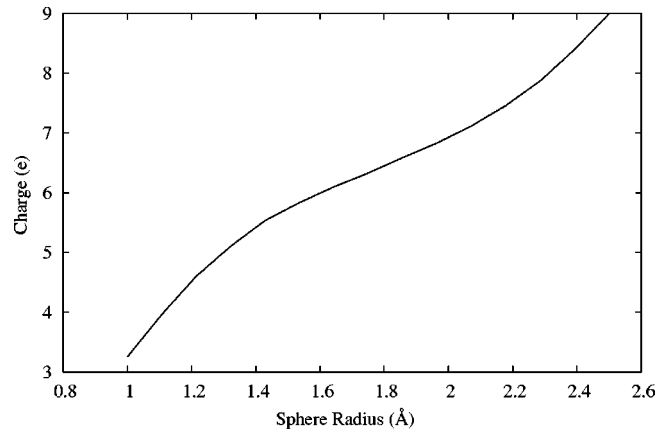


FIG. 5. Integrated charge around the Ba atom adsorbed at a **B** site at  $\frac{1}{16}$  ML coverage.

has a charge of  $+1.9e$ , recalling that our Ba pseudopotential has eight valence electrons. Regardless of binding site or coverage, the plots of charge density between adsorbed Ba atoms and surface Si atoms, and the plots of integrated charge around the Ba atoms are nearly identical. Even at a full monolayer of coverage, the Ba atoms still have a radius of  $\sim 1.7 \text{ \AA}$  with a charge of  $+1.6e$ . When bonding at the **H** site, the Ba adatom touches the four Si atoms at the corners of that site. When it has adsorbed at the **B** site, the Ba atom touches the four Si atoms at the corners, and the two Si atoms in the second layer. The charges of the Si atoms are difficult to integrate because of poor symmetry, but it appears that the charge from the Ba adatoms is distributed throughout the upper layers of the Si slab.

To follow the growth of Ba on the Si surface, we started with the relaxed  $(4 \times 4)$  **B** and **H** sites, and added one more Ba atom at the other **B** and **H** sites to form all thirteen  $\frac{1}{8}$  ML combinations possible on the  $(4 \times 4)$  lattice. These 13 structures are shown in Figs. 6 and 7, and their binding energies are summarized in Table III. From these energies we see that if Ba was to first fill a **B** site, the next site most likely to become occupied would be the closest **B** site in the  $[110]$  (along dimer row) direction. (see pattern **BB** in Fig. 6).

Wang *et al.*<sup>14</sup> predicted that Ba should form chains along the  $[110]$  direction. This prediction was made from the combination of the strong binding potential for Ba in the valleys, and the highly anisotropic diffusion behavior favoring the  $[110]$  direction. Wang *et al.* concluded that Ba would fall into the valleys, and then migrate along the valleys to their preferred binding sights. Our findings support the idea that Ba would bunch together to form chains along the valleys. This appears to be the most favorable sparse coverage structure, but its observation has not been reported.

If we consider the random adsorption of Ba on a grid of **B** sites, it is more likely that nearby Ba adatoms will be in an adjacent valley than in the same valley. Considering the results of Wang *et al.*, Ba adatoms might migrate along the valleys until they can make stable structures which run in the  $[\bar{1}10]$  (across dimer row) direction. This type of formation, crooked chains of Ba atoms on the **B** sites in adjacent valleys running in the  $[\bar{1}10]$  direction, was observed by Hu *et al.*<sup>8</sup>

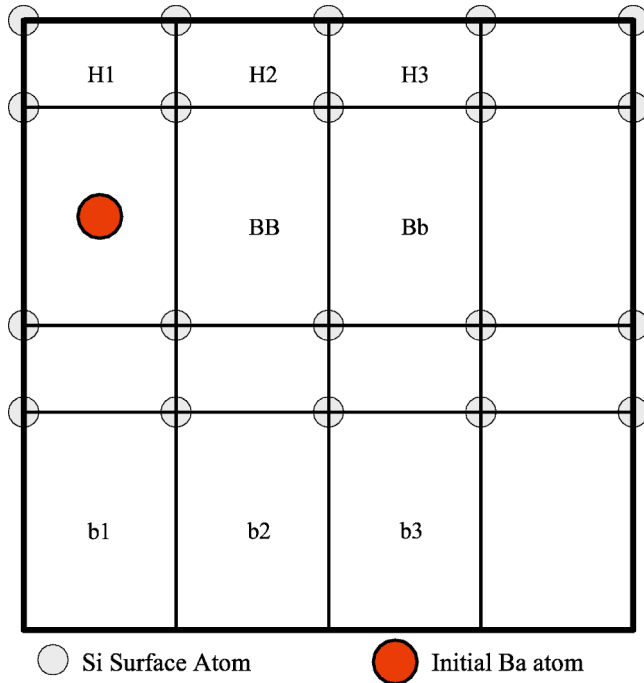


FIG. 6. (Color online) The patterns used to investigate the effect of a Ba atom adsorbed at a **B** site on the adsorption of a subsequent Ba atom. One atom was placed at the marked site and a second atom was placed at one of the labeled sites. Some of these combinations are identical to those shown in Fig. 7.

The most likely configuration of Ba adatoms on **B** sites in adjacent dimer rows is configuration **b2**, which [for the  $(4 \times 4)$  supercell] creates an infinitely long zig-zag chain of Ba atoms running in the  $[\bar{1}10]$  direction. It is important to note that to have a straight chain in the  $[\bar{1}10]$  direction (the **b1** structure) is the least favored combination of **B** sites. The energies for the **h1** and **h2** structures show a similar behavior, which indicates that at low coverage it is advantageous to have similar structures in adjacent valleys offset in the  $[110]$  direction.

Apart from the **H1** structure, configurations with two **B** sites are more likely than configurations involving **H** sites. It is difficult to tell whether this is because the **b1** structure has a low binding energy, or if **H-B** chains in the  $[\bar{1}10]$  direction are favorable structures. Repetition across valleys, and a  $(2 \times 4)$  supercell containing a **H-B** chain is discussed in the following section.

#### IV. $\frac{1}{4}$ AND $\frac{1}{3}$ ML COVERAGE

The binding energies of Ba on the four special sites at  $\frac{1}{4}$  ML listed in Table I were calculated using  $(4 \times 4)$  supercells with  $(4 \times 2)$  symmetry, and  $(2 \times 2)$  supercells. The  $(4 \times 4)$  supercells have the atoms across each valley shifted in the  $[110]$  direction, which is what the **b2** structure indicates as being preferred over the  $(2 \times 2)$  supercell, which is more like the **b1** structure. We see that at this coverage the **B** site is again the preferred site. For both the **B** and **H** sites the Si dimers have been stretched uniformly to  $2.41 \text{ \AA}$ , and are

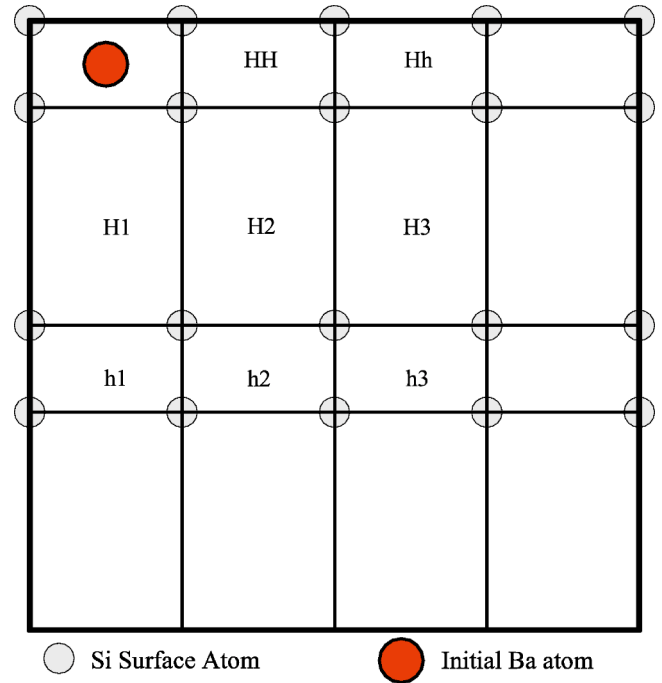


FIG. 7. (Color online) The patterns used to investigate the effect of a Ba atom adsorbed at a **H** site on the adsorption of a subsequent Ba atom. One atom was placed at the marked site and a second atom was placed at one of the labeled sites.

nearly symmetric. For the **D** and **C** sites only one dimer has been significantly affected (also stretched to  $\sim 2.4 \text{ \AA}$ ). It is interesting to note that the **C** site has become more competitive with the **H** site, and the **D** site has become substantially less favorable than the **C** site. This could be due to the cooperation of neighboring atoms in stretching the dimers. At the **C** site this would allow for better bonding of the Ba adatom, while at the **D** site this would cause partial breaking of the dimers. The binding energies for Ba adatoms at **B** and **H** sites in the  $(2 \times 2)$  supercell were 3.97 and 3.62 eV, respectively. From the charge densities in Fig. 8 we can see that when there is a Ba atom in the next valley without any offset they bond asymmetrically in the site. This asymmetry decreases the binding energy, thus making staggered structures more favorable.

A  $(2 \times 4)$  supercell containing an **H-B** chain in  $[\bar{1}10]$ ,

TABLE III. Binding energies per Ba adatom for the  $13 \frac{1}{8}$  ML configurations diagrammed in Figs. 6 and 7. Given from highest to lowest.

Pattern	BE	Pattern	BE
<b>BB</b>	4.43	<b>h2</b>	3.89
<b>Bb</b>	4.29	<b>H3</b>	3.88
<b>b2</b>	4.26	<b>H2</b>	3.87
<b>b3</b>	4.24	<b>Hh</b>	3.87
<b>H1</b>	4.10	<b>h1</b>	3.81
<b>b1</b>	3.97	<b>h3</b>	3.80
		<b>HH</b>	3.73

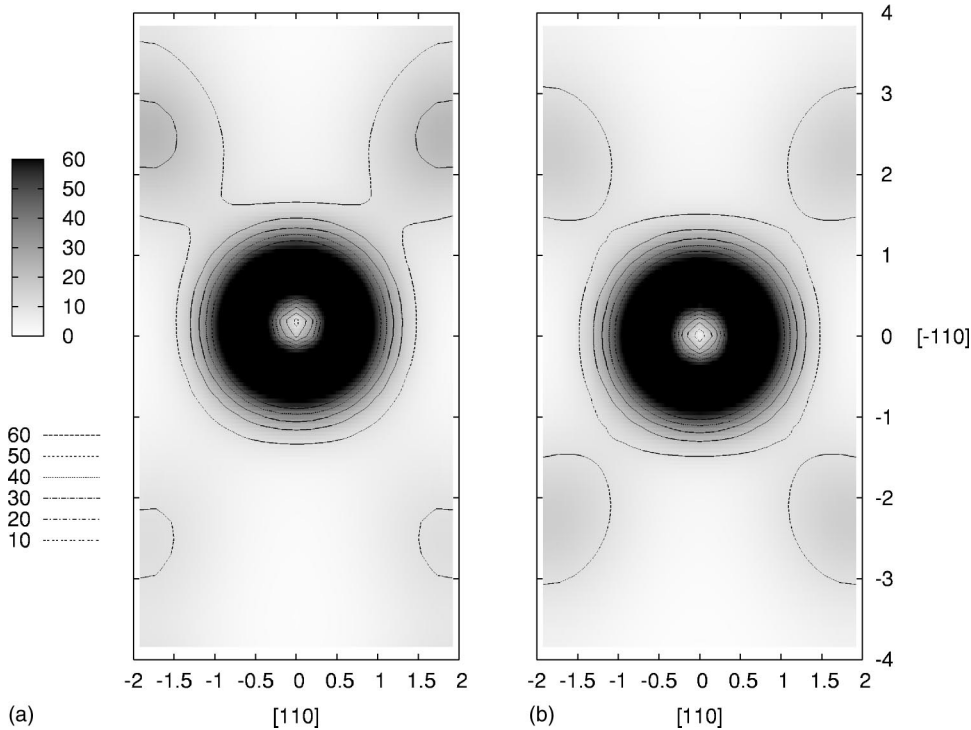


FIG. 8. The charge density in the (001) plane through the center of the adsorbed Ba atom above the **B** site for  $\frac{1}{4}$  ML coverage in the (a)  $(2 \times 2)$  and (b)  $(4 \times 4)$  supercells. The unit for the charge density is the same as in Fig. 4, hundredths of  $e/\text{\AA}^3$ .

and a  $(4 \times 4)$  supercell containing a **B** site chain in  $[110]$  were also investigated for  $\frac{1}{4}$  ML coverage, and the binding energy per Ba adatom were respectively found to be 3.92 and 3.80 eV. The **H-B** chain is competitive with the  $(2 \times 2)$  **B** site structure, but this type of chain would quickly break to form the  $(4 \times 2)$  **B** site structure. The **B** site chain is considerably less favorable than the other **B** site structures. Unlike the structures at higher coverages, the “2” part of the favorable  $\frac{1}{4}$  ML symmetry is in the  $[110]$  direction.

Using a  $(2 \times 3)$  supercell, we investigated the three possible combinations of **H** and **B** sites that could lead to the observed  $(2 \times 3)$  ordered phase at  $\frac{1}{3}$  ML coverage; the **BB**, **HB**, and **HH** structures shown in Fig. 9, which, respectively, yielded binding energies per Ba atom of 4.06, 4.01, and 3.49 eV. Again, we see that Ba atoms occupying **B** sites is the most favorable structure. It is somewhat surprising to see

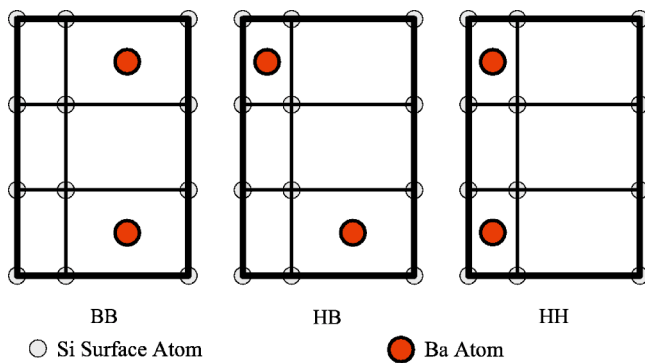


FIG. 9. (Color online) Top view of supercells used to investigate the possible  $(2 \times 3)$  structures at  $\frac{1}{3}$  ML.

that the **HB** structure is competitive with the **BB** structure, especially considering the relatively poor binding energy of **HH**. In both the **HH** and **BB** structures the neighboring Ba atoms sit asymmetrically in their sites, slightly pushed away from each other. Two obvious reason for this are the rather large size of the Ba atoms, which is comparable to the distance between neighboring sites, and their strong positive charge. The relaxed **BB** configuration is shown in Fig. 10, from which we can see that the Ba atoms are displaced by 0.33 Å from the center of the site. In the **BB** case, the Ba atoms are adsorbed at a height of 2.50 Å above the second Si layer, or 1.16 Å above the bulk-projected ideal surface. These findings are in good qualitative agreement with the experimental conclusions of Herrera-Gómez *et al.*,<sup>12</sup> who studied the geometry of the  $\frac{1}{3}$  ML  $(2 \times 3)$  surface and found that the Ba atoms were adsorbed at **B** sites, pushed 0.12 Å away from the center of the site, and were located at 1.55 Å above the bulk-projected ideal surface. In the **BB** structure we found that only the common dimer between two adsorbed Ba atoms, labeled in Fig. 10, was symmetric at a height of 0.11 Å above the projected surface, while the other dimers have reduced their buckling to 3.7° with a length of 2.37 Å.

## V. HALF MONOLAYER COVERAGE

From the lower coverages we know that Ba adsorbs preferentially on the **B** site, followed by adsorption on the **H** site. Furthermore, we have seen from  $\frac{1}{3}$  ML patterns that Ba atoms might adsorb in combinations of **B** and **H** sites if this allows for the Ba atoms to make accommodations for their size and charge. This leads to many possible combinations of  $(2 \times N)$  symmetries. To study  $\frac{1}{2}$  ML coverage we first calcu-

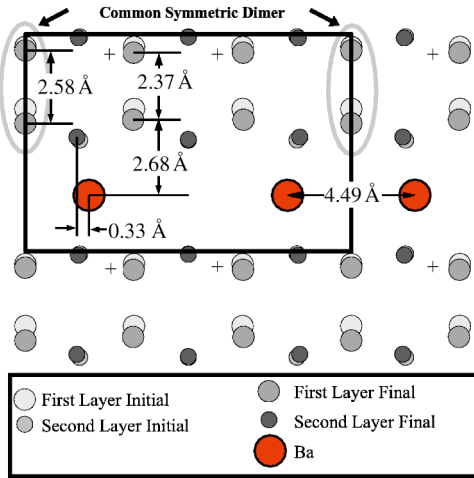


FIG. 10. (Color online) The top view and geometry of the lowest energy  $\frac{1}{3}$  ML structure with  $(2 \times 3)$  symmetry. The positions of the clean  $p(2 \times 1)$  surface are shown along with those of the Ba covered surface. The high Si atom in each dimer is labeled with +. The dimer labeled as “common dimer” is symmetric, while the other dimers are asymmetric. The box outlines the  $(2 \times 3)$  supercell.

lated the binding energies of the symmetry sites using a  $(2 \times 1)$  supercell. These energies are listed in Table I. The **B** site has the highest binding energy at this coverage, and the energy differences among all four sites are significant. The structural parameters pertinent to the **B** and **H** sites are diagrammed in Figs. 11 and 12, respectively. Note that the dimers have been stretched to  $2.50 \text{ \AA}$ , but are still intact. There is no evidence of any buckling in the dimers. Herrera-Gómez *et al.*<sup>12</sup> studied adsorption at  $\frac{1}{2}$  ML with  $(2 \times 1)$  symmetry, and found that Ba atoms adsorbed at the **B** sites,  $1.22 \text{ \AA}$  above the bulk-projected surface. We found that Ba atoms are located at the **B** site  $1.18 \text{ \AA}$  above the bulk-projected surface, and  $1.09 \text{ \AA}$  above the dimers, which is consistent with the experiment. We calculated the band structure for the **B** site, and found the valence and conducting bands to just overlap, destroying the gap. Unfortunately, DFT tends to underestimate band gaps, so in truth  $\frac{1}{2}$  ML coverage could just as easily be semiconducting.

Due to the prevalence of the **B** site over the **H** site we used  $(2 \times N)$  symmetries in which as many Ba atoms as possible were adsorbed on the **B** site, with a remaining atom adsorbed on the **H** site. This resulted in the  $(2 \times 1)$  through  $(2 \times 6)$  symmetries shown in Fig. 13. The energies of these structures are given in Table IV. We note that, contrary to the published findings, the  $(2 \times 1)$  symmetry is not the preferred symmetry at  $\frac{1}{2}$  ML. The preferred symmetry is  $(2 \times N)$ , where  $N=3-6$ . Recalling that the possible error between different symmetries due to **k** point sampling is  $\sim 10 \text{ meV}$ , one may conclude that the optimal number of Ba atoms per segment in an interrupted chain along the valley is about four to five atoms. This allows the Ba atoms to accommodate their large size and charge while adsorbing at the preferred **B** site. The near degeneracy of these different symmetries along the dimer rows accounts for the reports of poor ordering in the  $\frac{1}{2}$  ML structures.<sup>7-11</sup>

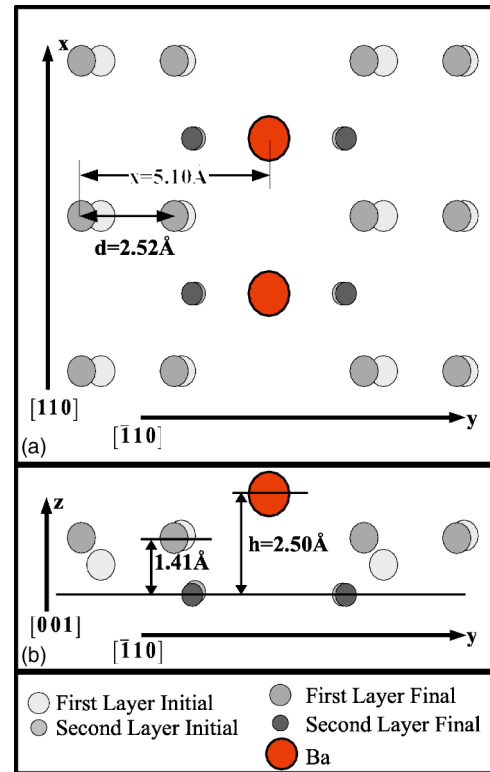


FIG. 11. (Color online) Top view (a) and cross sectional view down the dimer rows (b) for the  $(2 \times 1)$   $\frac{1}{2}$  ML surface with Ba atoms adsorbed at the **B** sites.

A wavy ordering was observed at  $\frac{1}{2}$  ML by Ojima *et al.*,<sup>10</sup> and a possible unit cell with buckled Ba dimers in the  $[110]$  direction (along the valley) was used by Ojima *et al.* to explain the wavy ordering. The wavy ordering indicates that the pattern of Ba atoms in one valley is repeated in the  $[\bar{1}10]$  direction (across valleys), and offset by one unit cell in the  $[110]$  direction. We calculated the energy and structure for the unit cell proposed by Ojima *et al.*, and investigated the ordering in the  $[\bar{1}10]$  direction by using two of the  $(2 \times 4)$  chains shown in Fig. 13 in a  $(4 \times 4)$  supercell offset by 0, 1, and 2 unit cells in the  $[110]$  direction. We made several attempts at creating the  $[110]$  Ba dimers, both in  $(2 \times 4)$  and  $(4 \times 4)$  supercells, all of which relaxed into a nearly perfect  $(2 \times 1)$  unit cell. From the sections on sparse and  $\frac{1}{4}$  ML coverages we would have expected to find that having an offset would be the most preferred ordering, instead we found that having the  $(2 \times 4)$  pattern repeat without any offset gave the highest total binding energy, followed by the single and double offsets at 0.29 and 0.52 eV lower total binding energies respectively. This behavior is the opposite of what we found in the  $\frac{1}{8}$  ML filling and  $\frac{1}{4}$  ML structures, and is contradictory to the work of Ojima *et al.* At half monolayer coverage, Ba atoms sit symmetrically in the center of their sites, regardless of what happens in the next valley. While this might explain the high degree of ordering across dimer rows in the  $(2 \times 3)$  phase at  $\frac{1}{3}$  ML, it does not explain the wavy structure observed at  $\frac{1}{2}$  ML. Given the small energy difference between the zig-zag and straight structures, it is possible that single offsets at  $\frac{1}{2}$  ML are only

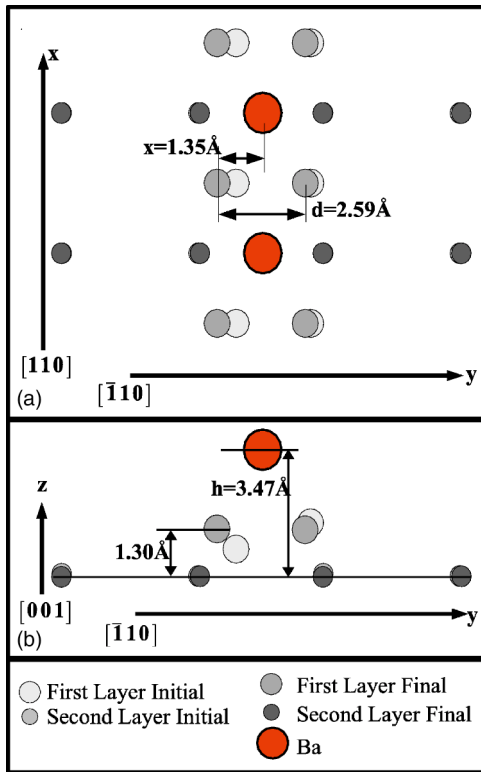


FIG. 12. (Color online) Top view (a) and cross sectional view down the dimer rows (b) for the  $(2 \times 1)$   $\frac{1}{2}$  ML surface with Ba atoms adsorbed at the **H** sites.

favorable for long runs in the  $[\bar{1}10]$  direction without reversing the direction of the offset, as might be indicated from the observations of Ojima *et al.*, as opposed to the zig-zag ordering of our  $(4 \times 4)$  supercell, but testing this would require an  $(8 \times 4)$  supercell, which was beyond our computational ability.

VI. ONE MONOLAYER COVERAGE

We tested both  $(2 \times 2)$  and  $(2 \times 4)$  symmetries for  $\frac{3}{4}$  ML coverage, filling the **B** sites in a  $(2 \times 1)$  fashion and adding

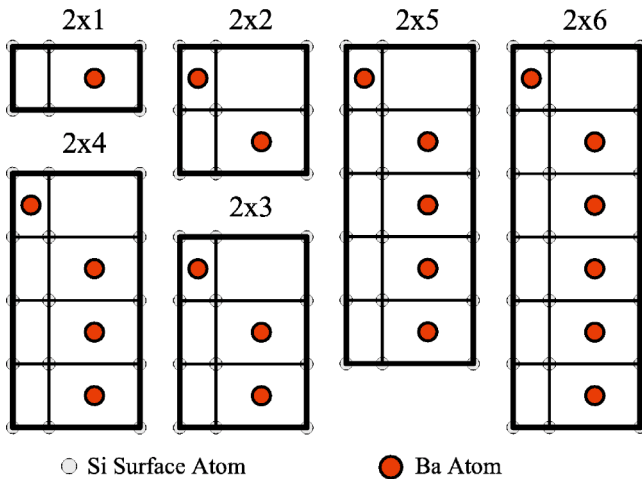


FIG. 13. (Color online) Top view of supercells used to investigate the possible  $(2 \times N)$  structures at  $\frac{1}{2}$  ML.

TABLE IV. Binding energies per Ba adatom for the six  $(2 \times N)$  configurations at  $\frac{1}{2}$  ML coverage.

Structure	BE	Structure	BE
$(2 \times 1)$	3.90	$(2 \times 4)$	4.00
$(2 \times 2)$	3.80	$(2 \times 5)$	3.99
$(2 \times 3)$	4.02	$(2 \times 6)$	3.97

the next Ba atoms to the **H** sites. We found the  $(2 \times 2)$  phase was preferred over the  $(2 \times 4)$  phase by 0.22 eV for the entire  $(2 \times 4)$  supercell. The structure of the  $(2 \times 2)$  phase is shown in Fig. 14. For the  $(2 \times 2)$  symmetry, the Si dimers are perfectly symmetric and are at a height of 1.37 Å above the second plane of Si. The heights of the Ba atoms at the **H** sites have increased to 3.83 Å above the second Si plane, and the heights of the Ba atoms at the **B** sites alternate between

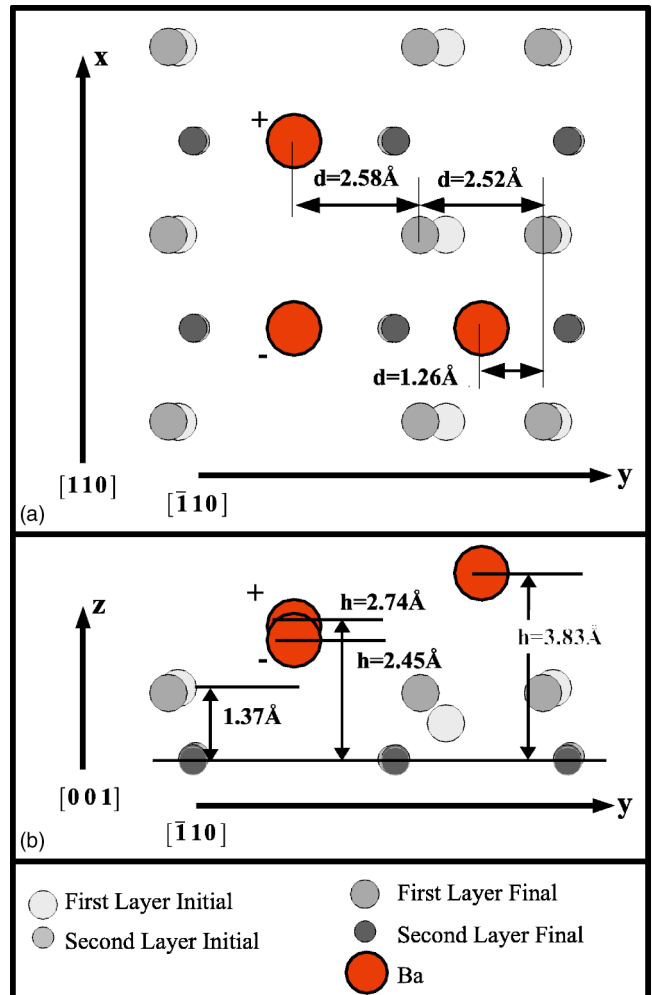


FIG. 14. (Color online) The  $(2 \times 2)$  phase of  $\frac{3}{4}$  ML coverage. Frame a shows the top view and frame b shows the view looking down the dimer rows. Notice that the Si dimers are symmetric at this coverage, while the second layer is slightly distorted. The Ba atoms adsorbed at the **B** sites are not at the same height. The atom labeled + is higher than the other Ba atom (labeled -), which is pushed down by the Ba atom adsorbed at the **H** site.

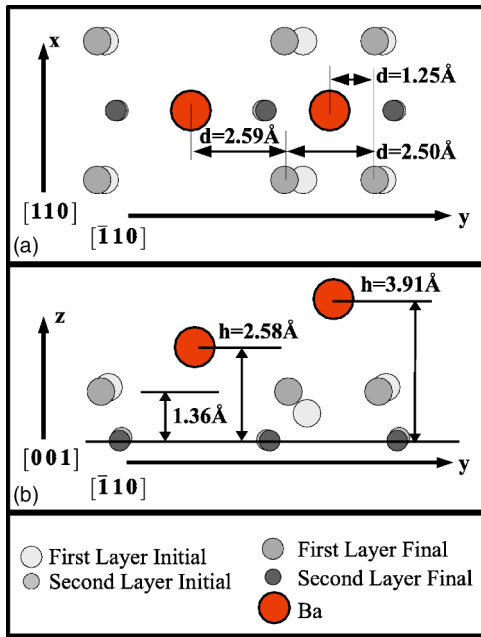


FIG. 15. (Color online) Geometry of the  $(2 \times 1)$  full monolayer covered surface with Ba adsorbed on **B** and **H** sites. Frame a shows the top view and frame b shows the view looking down the dimer rows.

2.45 and 2.74 Å, with the lower height being in the  $\langle \bar{1}10 \rangle$  direction between the occupied **H** sites. The dimers remain unbroken at a length of 2.50 Å. Cho *et al.*<sup>13</sup> studied a surface at 0.7 ML, and found that Ba adsorbed at **B** sites, and then randomly at the **H** sites. They found the height of Ba atoms at the **B** and **H** sites to be respectively 3.0 and 3.5 Å above the second layer of Si.

At full ML coverage there is one Ba atom at every **B** site, and another at either **D** or **H** sites. The  $(2 \times 1)$  combination of **B** and **H** sites, shown in Fig. 15, is preferred by a modest excess binding energy of 0.07 eV for the entire  $(2 \times 1)$  supercell over the  $(2 \times 1)$  combination of **B** and **D** sites. The Si dimers are symmetric and intact with a length of 2.50 Å at a height of 1.36 Å above the second Si layer, which is also the bulk layer-layer distance. All Si layers are at their bulk projected heights. The **H** and **B** sites are at  $\sim 3.9$  Å and  $\sim 2.6$  Å above the second Si layer, respectively. We calculated the energy with and without broken Si dimers and found that at full coverage each dimer still yields an energy gain, albeit reduced to 0.2 eV per dimer. The binding energy for each Ba atom has dropped to roughly 3 eV. The sequence of Figs. 16, 17, and 18 shows the charge density of the full ML covered surface in (001) planes at three different heights centered on the **H** site, with the planes going through the Ba atoms adsorbed at the **H** sites and **B** sites, and the Si dimers respectively. From Figs. 16 and 17 it is evident that there is very little charge between adsorbed Ba atoms. You can also see that the radius of the Ba atoms is  $\sim 1.7$  Å. This makes sense considering the ionic nature of the bonding. Figure 18 shows that there is still bonding between Si atoms creating Si dimers. The band structure for full monolayer coverage

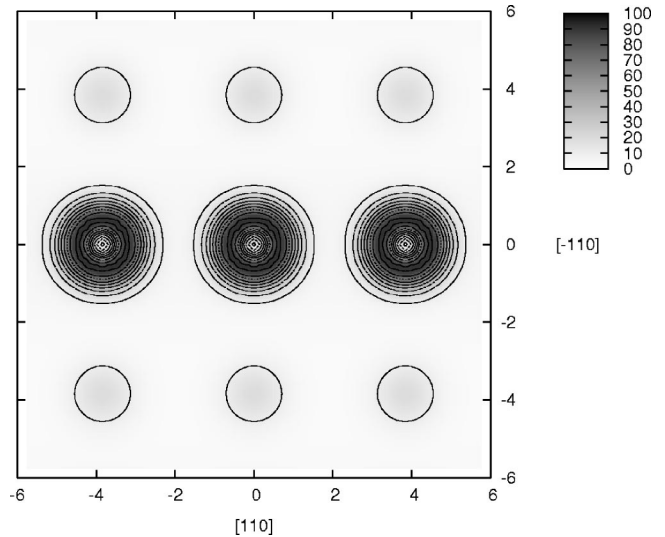


FIG. 16. Charge density plot in the (001) plane centered on the **H** site through the center of the adsorbed Ba atoms at the **H** sites. The unit for the charge density is the same as in Fig. 4, hundredths of  $e/\text{Å}^3$ . Visible in the plot are the Ba atoms at the **H** sites, and the tops of the Ba-atoms at the **B** sites.

shows a definite lack of a band gap, indicating a metallic surface.

## VII. CONCLUSIONS

At low coverage, Ba adatoms adsorb onto the Si(001) surface at valley bridge (**B**) sites, where they form ionic bonds between the four Si surface atoms at the corners of the site and the two Si atoms in the second layer beneath the site. As growth of the Ba layer progresses, the additional Ba at-

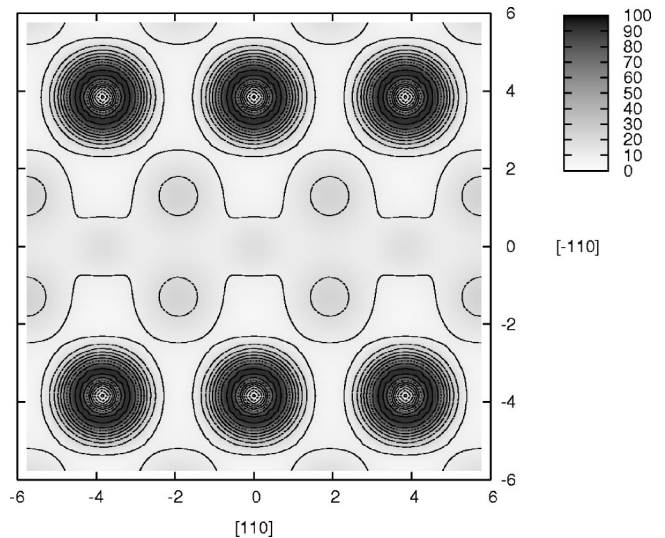


FIG. 17. Charge density plot in the (001) plane centered on the **H** site through the center of the Ba atoms adsorbed at the **B** sites. The unit for the charge density is the same as in Fig. 4, hundredths of  $e/\text{Å}^3$ . Visible in the plot are the Ba atoms at the **B** sites, the bottoms of the Ba atoms at the **H** sites, and the tops of the Si dimers.

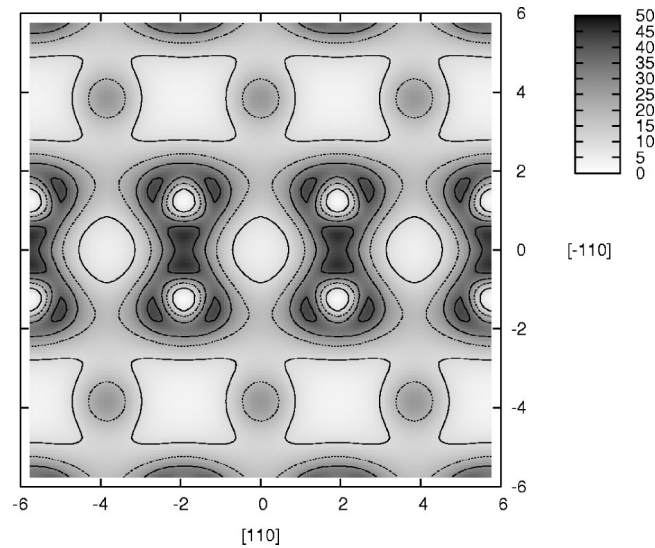


FIG. 18. Charge density plot in the (001) plane centered on the **H** site through the plane of the Si dimers. The unit for the charge density is the same as in Fig. 4, hundredths of  $e/\text{\AA}^3$ . Visible in the plot are the Si dimers, and the bottoms of the Ba atoms at the **B** sites.

oms should start adsorbing at valley bridge sites adjacent to Ba atoms that were already adsorbed. This indicates a possibility of forming chains in the  $[110]$  direction along the valleys, except that Ba's large size and positive charge causes these chains to break. From the results at  $\frac{1}{2}$  ML, it appears that chains along the  $[110]$  direction would break after running four to five atoms, forming interrupted chains. Barium might also form crooked "chains" which run along the  $[\bar{1}10]$  direction across dimer rows. But these chains are not the preferred structure, and most likely result from the random distribution of Ba atoms into adjacent valleys, followed

by their rapid migration along the valleys to form more stable across-valley structures. Also, these chains are sparse structures with relatively large distances between neighboring Ba atoms, which makes them unlikely to be electronically significant. Up to  $\frac{1}{4}$  ML coverage, the pattern of Ba atoms in neighboring valleys should be offset, but this changes by  $\frac{1}{3}$  ML coverage.

Barium atoms almost exclusively occupy the valley bridge sites for coverages up to  $\frac{1}{3}$  ML, but after this coverage Ba starts to occupy hollow (**H**) sites to avoid stresses caused by their large radii and positive charges. At  $\frac{1}{2}$  ML,  $(2 \times 1)$  is not the preferred symmetry. The structure is instead a mixture of 2, 3, 4, and 5 atom long chain segments of Ba atoms running in the  $[110]$  direction (along the valley) adsorbed on **B** sites, which are interrupted by Ba atoms at **H** sites. There is good indication that the pattern of Ba atoms should repeat in the  $[\bar{1}10]$  direction without any offset in  $[110]$ . The band structure at  $\frac{1}{2}$  ML coverage indicates the possibility of a metallic surface, but limitations in DFT cause difficulty in making a determination. As coverage increases the valley bridge sites are filled and Ba atoms start to occupy hollow sites. At full ML coverage the Si dimers remain intact and are no longer buckled. The band structure at full monolayer coverage shows the lack of a band gap, indicating a conducting surface. Barium atoms do not form Ba-Ba dimers at any coverage we investigated.

*Note added in proofs:* Recently, we saw a theoretical paper<sup>25</sup> dealing with Sr on Si(001) which shows complementary and similar properties to Ba since Sr is an *s*-shell atom in the row above Ba.

#### ACKNOWLEDGMENTS

For exploration of the charge density, and the creation of the charge density plots we used the package LEV00 created by Lev Kantorovich.<sup>24</sup>

\*Electronic address: ipbatra@uic.edu

<sup>1</sup>W.C. Fan and A. Ignatiev, Surf. Sci. **253**, 297 (1991).

<sup>2</sup>D. Vlachos, M. Kamaratos, and C. Papageorgopoulos, Solid State Commun. **90**, 175 (1994).

<sup>3</sup>T. Urano, K. Tamiya, K. Ojima, S. Hongo, and T. Kanaji, Surf. Sci. **357-358**, 459 (1996).

<sup>4</sup>Y. Takeda, T. Urano, T. Ohtani, K. Tamiya, and S. Hongo, Surf. Sci. **402-404**, 692 (1998).

<sup>5</sup>J.S. Kim, K.W. Ihm, C.C. Hwang, H.S. Kim, Y.K. Kim, C. Lee, and C.Y. Park, Jpn. J. Appl. Phys. **38**, 6479 (1999).

<sup>6</sup>X. Hu, C.A. Peterson, D. Sarid, Z. Yu, J. Wang, D.S. Marshall, R. Droopad, J.A. Hallmark, and W.J. Ooms, Surf. Sci. **426**, 69 (1999).

<sup>7</sup>X. Yao, X. Hu, D. Sarid, Z. Yu, J. Wang, D.S. Marshall, R. Droopad, J.K. Abrokwhah, J.A. Hallmark, and W.J. Ooms, Phys. Rev. B **59**, 5115 (1999).

<sup>8</sup>X. Hu, X. Yao, C.A. Peterson, D. Sarid, Z. Yu, J. Wang, D.S. Marshall, R. Droopad, J.A. Hallmark, and W.J. Ooms, Surf. Sci. **445**, 256 (2000).

<sup>9</sup>X. Hu, X. Yao, C.A. Peterson, D. Sarid, Z. Yu, J. Wang, D.S. Marshall, J.A. Curless, J. Ramdani, R. Droopad, J.A. Hallmark,

and W.J. Ooms, Surf. Sci. Lett. **457**, L391 (2000).

<sup>10</sup>K. Ojima, M. Yoshimura, and K. Ueda, Phys. Rev. B **65**, 075408 (2002).

<sup>11</sup>K. Ojima, M. Yoshimura, and K. Ueda, Surf. Sci. **491**, 169 (2001).

<sup>12</sup>A. Herrera-Gómez, P. Pianetta, D. Marshall, E. Nelson, and W.E. Spicer, Phys. Rev. B **61**, 12 988 (2000).

<sup>13</sup>W.S. Cho, J.Y. Kim, S.S. Kim, D.S. Choi, K. Jeung, I.W. Lyo, C.N. Whang, and K.H. Chae, Surf. Sci. Lett. **476**, L259 (2001).

<sup>14</sup>J. Wang, J.A. Hallmark, D.S. Marshall, W.J. Ooms, P. Ordejn, J. Junquera, D. Sánchez-Portal, E. Artacho, and J.M. Soler, Phys. Rev. B **60**, 4968 (1998).

<sup>15</sup>G.V. Benemanskaya, D.V. Daïneka, and D.E. Frank-Kamenetskaya, J. Exp. Theor. Phys. **87**, 1167 (1998).

<sup>16</sup>G. Kresse and J. Hafner, Phys. Rev. B **47**, R558 (1993).

<sup>17</sup>G. Kresse and J. Furthmüller, Phys. Rev. B **54**, 11 169 (1996).

<sup>18</sup>H.J. Monkhorst and J.D. Pack, Phys. Rev. B **13**, 5188 (1976).

<sup>19</sup>D. Vanderbilt, Phys. Rev. B **41**, 7892 (1990); G. Kresse and J. Hafner, J. Phys.: Condens. Matter **6**, 8245 (1994).

<sup>20</sup>J.P. Perdew and Y. Wang, Phys. Rev. B **46**, 6671 (1992).

<sup>21</sup>A. Ramstad, G. Brocks, and P.J. Kelly, Phys. Rev. B **51**, 14 504 (1995).

- <sup>22</sup>P. Sen, S. Ciraci, I.P. Batra, C.H. Grein, and S. Sivananthan, Surf. Sci. **519**, 79 (2002).
- <sup>23</sup>I.P. Batra, Phys. Rev. B **43**, 12 322 (1991).
- <sup>24</sup>L.N. Kantorovich, *User Friendly Visualization Program for Planewave ab initio DFT Codes CASTEP/CETEP/VASP*, 1996–2002 (unpublished).
- <sup>25</sup>C.R. Ashman, C.J. Först, K. Schwarz, and P.E. Blöchl, Phys. Rev. B **59**, 075309 (2004).